

# Raman scattering study of spin-density-wave-induced anisotropic electronic properties in $A\text{Fe}_2\text{As}_2$ ( $A = \text{Ca}, \text{Eu}$ )

W. -L. Zhang,<sup>1,2</sup> Z. P. Yin,<sup>2</sup> A. Ignatov,<sup>2</sup> Z. Bukowski,<sup>3,4</sup> Janusz Karpinski,<sup>3</sup>  
Athena S. Sefat,<sup>5</sup> H. Ding,<sup>1,6</sup> P. Richard,<sup>1,6</sup> and G. Blumberg<sup>2,7,\*</sup>

<sup>1</sup>*Beijing National Laboratory for Condensed Matter Physics and Institute of Physics,  
Chinese Academy of Sciences, Beijing, 100190, China*

<sup>2</sup>*Department of Physics & Astronomy, Rutgers University, Piscataway, New Jersey 08854, USA*

<sup>3</sup>*Laboratory for Solid State Physics, ETH Zurich, 8093 Zurich, Switzerland*

<sup>4</sup>*Institute of Low Temperature and Structure Research,*

*Polish Academy of Sciences, P.O. Box 1410, 50-422 Wrocław, Poland*

<sup>5</sup>*Materials Science and Technology Division, Oak Ridge National Laboratory, Oak Ridge, Tennessee 37831-6114, USA*

<sup>6</sup>*Collaborative Innovation Center of Quantum Matter, Beijing, China*

<sup>7</sup>*National Institute of Chemical Physics and Biophysics, Akadeemia tee 23, 12618 Tallinn, Estonia*

We present a polarization-resolved and temperature-dependent Raman scattering study of  $A\text{Fe}_2\text{As}_2$  ( $A = \text{Ca}, \text{Eu}$ ). In the spin-density-wave (SDW) phase, spectral weight redistribution is observed in the fully symmetric and non-symmetric scattering channels at different energies. An anisotropic Raman response is observed in the fully symmetric channel in spontaneously detwinned  $\text{CaFe}_2\text{As}_2$  samples. We calculate the orbital-resolved electronic structures using a combination of density functional theory and dynamical mean field theory (DFT+DMFT). We identify the electronic transitions corresponding to these two spectral features and find that the anisotropic Raman response originates from the lifted degeneracy of the  $d_{xz}/d_{yz}$  orbitals in the broken symmetry phase.

The parent and underdoped compounds of the 122 family ( $A\text{Fe}_2\text{As}_2$ ) of iron-pnictide superconductors harbor an antiferromagnetic ground state with a collinear stripe spin order of Fe ions. The formation of a spin-density-wave (SDW) order at a temperature  $T_{SDW}$  is accompanied by a tetragonal to orthorhombic structural distortion in which the  $C_4$  rotational symmetry is broken<sup>1</sup>. Although the lattice distortion is small, the electronic anisotropy can be large<sup>2</sup>. For a strain-free sample, a twin domain structure with a typical dimension of a few micrometers usually forms with orthogonally aligned antiferromagnetic directions<sup>3</sup>. In many macroscopic symmetry-sensitive experiments, the response along the antiferromagnetic and ferromagnetic directions can be mixed and averaged. However, strongly anisotropic responses in the  $dc$  and  $ac$  electrical conductivity<sup>4-6</sup>, the thermoelectric power<sup>7</sup> and the magnetic susceptibility<sup>8</sup> along the two orthogonal directions, as well as in the on-site energy splitting of the  $d_{xz}$  and  $d_{yz}$  orbitals<sup>9</sup>, have been reported for samples completely or partially detwinned following the application of a uniaxial strain or stress<sup>4,10</sup>, or an in-plane magnetic field<sup>11</sup>.

Electronic Raman scattering is an inelastic light scattering process that traces the density-density correlation function driven by the incident and scattered lights. With a proper choice of light polarization, it can separate states or collective excitations associated with certain symmetries belonging to the irreducible representations of the point group of a particular crystal<sup>12</sup>. For example, the  $d$ -wave superconducting gap in cuprates results in a  $\omega^3$  Raman response in the nodal direction and a linear Raman response in the anti-nodal direction<sup>13,14</sup>. In the iron-pnictides, the nematic fluctuations of the XY symmetry is observed in the tetragonal phase with cross-polarized light along the Fe-As directions<sup>15-19</sup>. There-

fore, it is of interest to study the Raman response for excitations of different symmetries across the structural and magnetic phase transition.

In this paper, we present polarization-resolved electronic Raman measurements of the iron-pnictide parent compound  $A\text{Fe}_2\text{As}_2$  ( $A = \text{Ca}, \text{Eu}$ ). We observe two spectral features with different symmetries below  $T_{SDW}$ . One feature is a coherence peak in the fully symmetric channel that was previously assigned to the formation of a SDW gap near the  $M(\pi/a, 0, 0)$  point<sup>20</sup>. Using symmetry analysis of a detwinned sample, as well as combination of density functional theory and dynamical mean field theory (DFT+DMFT) calculations<sup>21,22</sup> above and below  $T_{SDW}$ , we show that this feature is an intra-orbital transition near the  $Z(0, 0, 2\pi/c)$  point. In the non-symmetric channel, we identify an additional small peak at lower frequency that originates from the lifted degeneracy of the  $d_{xz}$  and  $d_{yz}$  orbital at the  $\Gamma$  point.

The  $\text{CaFe}_2\text{As}_2$  and  $\text{EuFe}_2\text{As}_2$  samples employed in this study have been synthesized by Sn and Fe-As flux methods described in Refs.<sup>23,24</sup>.  $\text{CaFe}_2\text{As}_2$  goes through a second order phase transition at 170 K whereas  $\text{EuFe}_2\text{As}_2$  goes through a first order phase transition at 175 K. The high-temperature tetragonal structure belongs to the space group  $I4/mmm$  (point group  $D_{4h}$ ) and the low-temperature orthorhombic structure belongs to the space group  $Fmmm$  (point group  $D_{2h}$ ). Freshly cleaved  $\text{CaFe}_2\text{As}_2$  and  $\text{EuFe}_2\text{As}_2$  single-crystals have been measured in a quasi-back scattering geometry from the  $ab$  surface. The 476 and 647 nm laser beam of a  $\text{Kr}^+$  ion laser with a total incident power smaller than 15 mW were focused on a  $50 \times 125 \mu\text{m}^2$  spot on the sample surface. The scattered light was analyzed by a triple grating spectrometer and collected by a liquid  $\text{N}_2$ -cooled CCD detector. The data were corrected for the spectral re-

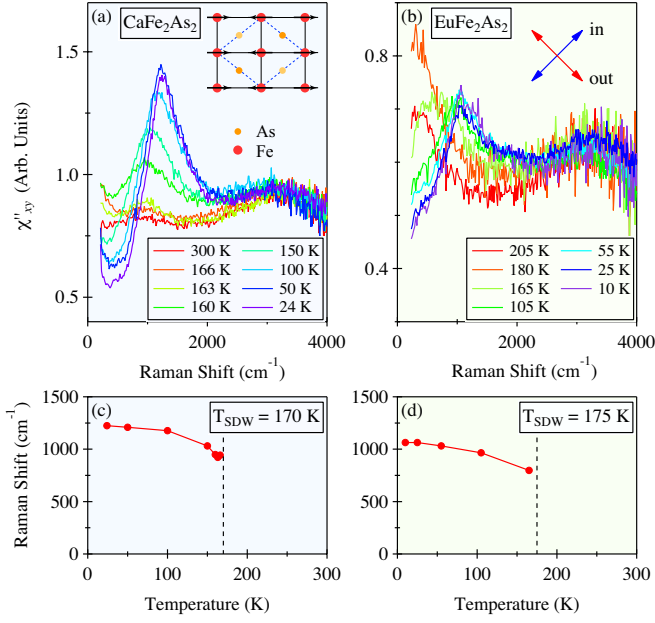


FIG. 1. (Color online) (a) Temperature dependence of the Raman response of untwinned  $\text{CaFe}_2\text{As}_2$  in the  $XY$  polarization configuration corresponding to the  $B_{2g}(D_{4h})/A_g(D_{2h})$  symmetry channel, recorded with a 647 nm laser excitation. The inset illustrates one Fe-As layer of the 4-Fe unit cell in the low-temperature phase, along with the Fe magnetic moments (red arrow). Dark and light colors denote the sign of the wave functions. (b) Same as (a) but for twinned  $\text{EuFe}_2\text{As}_2$ . The inset shows the incident and scattered light polarizations with respect to the lattice orientation in the inset of (a). (c) and (d) Frequency of the coherence peak as a function of temperature for  $\text{CaFe}_2\text{As}_2$  and  $\text{EuFe}_2\text{As}_2$ , respectively.

sponse of the system at different wavelengths<sup>25</sup>. The polarization configuration ( $e^I e^S$ ) is defined by the polarization of the incident and scattered photons,  $e^I$  and  $e^S$ , respectively. The polarization vectors  $x = [110]$  and  $y = [\bar{1}10]$  are along the nearest Fe-Fe bonds corresponding respectively to the antiferromagnetic (AFM) and ferromagnetic (FM) directions in the SDW phase, and  $X = [100]$  and  $Y = [010]$  form a  $45^\circ$  angle with them.

In Fig. 1, we show the Raman response of  $\text{CaFe}_2\text{As}_2$  and  $\text{EuFe}_2\text{As}_2$  for the  $XY$  scattering geometry at various temperatures above and below  $T_{SDW}$ . We observe a spectral weight transfer from low-frequency to above  $800 \text{ cm}^{-1}$  with the development of a coherence peak. As indicated in Figs. 1(c) and 1(d), the coherence peak in  $\text{CaFe}_2\text{As}_2$  ( $\text{EuFe}_2\text{As}_2$ ) hardens from 920 (800)  $\text{cm}^{-1}$  to 1220 (1060)  $\text{cm}^{-1}$  from  $T_{SDW}$  to the lowest measured temperature. This spectral feature was previously assigned to the formation of a SDW gap<sup>20</sup>, which is accompanied by the appearance of a Dirac cone in the electronic structure<sup>26,27</sup>.

We performed polarization-dependent measurements on  $\text{CaFe}_2\text{As}_2$  and  $\text{EuFe}_2\text{As}_2$  samples. The electronic states in the vicinity of the Fermi level ( $E_F$ ) in the iron-

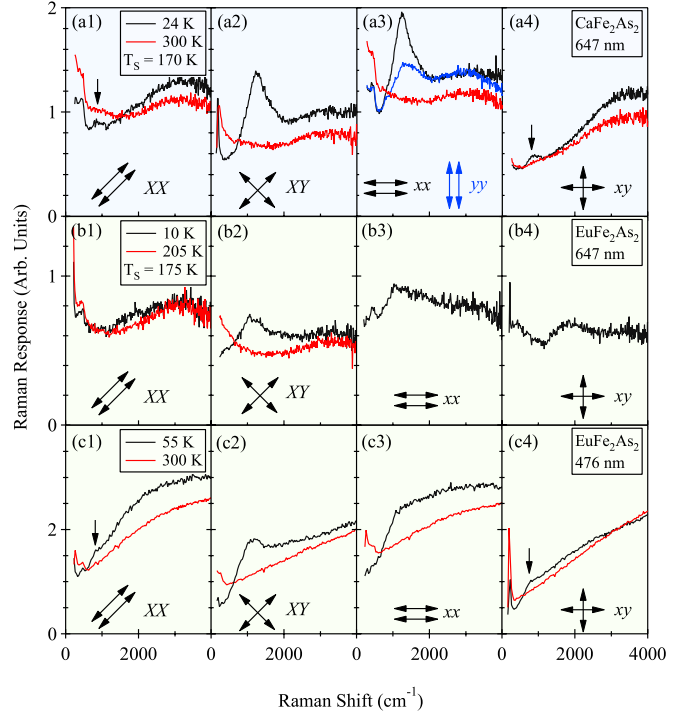


FIG. 2. (Color online) (a1)-(a4) Raman response of  $\text{CaFe}_2\text{As}_2$  measured with 647 nm laser excitation in different in-plane polarization configurations (denoted by the arrows) in the normal state (300 K, red) and in the detwinned SDW phase (24 K, black/blue). (b1)-(b4) Raman response of  $\text{EuFe}_2\text{As}_2$  in different in-plane polarization configurations in the normal state (205 K, red) and the twinned SDW state (10 K, black). (c1)-(c4) Same as (b1)-(b4) with the 476 nm laser excitation.

pnictides consists mainly of Fe 3d orbitals. Locally, these states decompose into  $A_{1g}$  ( $d_{z^2}$ ),  $B_{2g}$  ( $d_{x^2-y^2}$ ),  $B_{1g}$  ( $d_{xy}$ ) and two  $E_g$  ( $d_{xz}$ ,  $d_{yz}$ ) states, which behave differently under the symmetry operations of the  $D_{4h}$  group. We note that in the low-temperature SDW phase the crystal structure of  $\text{AFe}_2\text{As}_2$  is lowered to the  $D_{2h}$  group and some  $D_{4h}$  in-plane irreducible representations merge together, i.e.  $A_{1g}$  and  $B_{2g}$  merge into  $A_g$  while  $A_{2g}$  and  $B_{1g}$  merge into  $B_{1g}$ . Our results are displayed in Fig. 2. We first discuss the Raman responses obtained on  $\text{CaFe}_2\text{As}_2$  (first row in Fig. 2). At room temperature, we observe a continuum up to the highest measured frequency in all polarization configurations. Typically, a twinned orthorhombic structure forms upon cooling down the samples below  $T_{SDW}$ , as can be viewed under a microscope with crossed-polarized light<sup>3</sup>. To maximize the size of the domains, our samples were cooled down in two steps. At temperatures way above  $T_{SDW}$ , the samples were cooled at a rate higher than 60 K/hr. Upon approaching  $T_{SDW}$  though, this cooling rate was decreased below 1 K/hr. Using this procedure, a mono-domain in millimeter size formed in our  $\text{CaFe}_2\text{As}_2$  samples, which we confirmed using laser illumination with  $XY$  polarization. In Figs. 2(a1)-(a4) we show the Raman scattering intensity of a  $\text{CaFe}_2\text{As}_2$

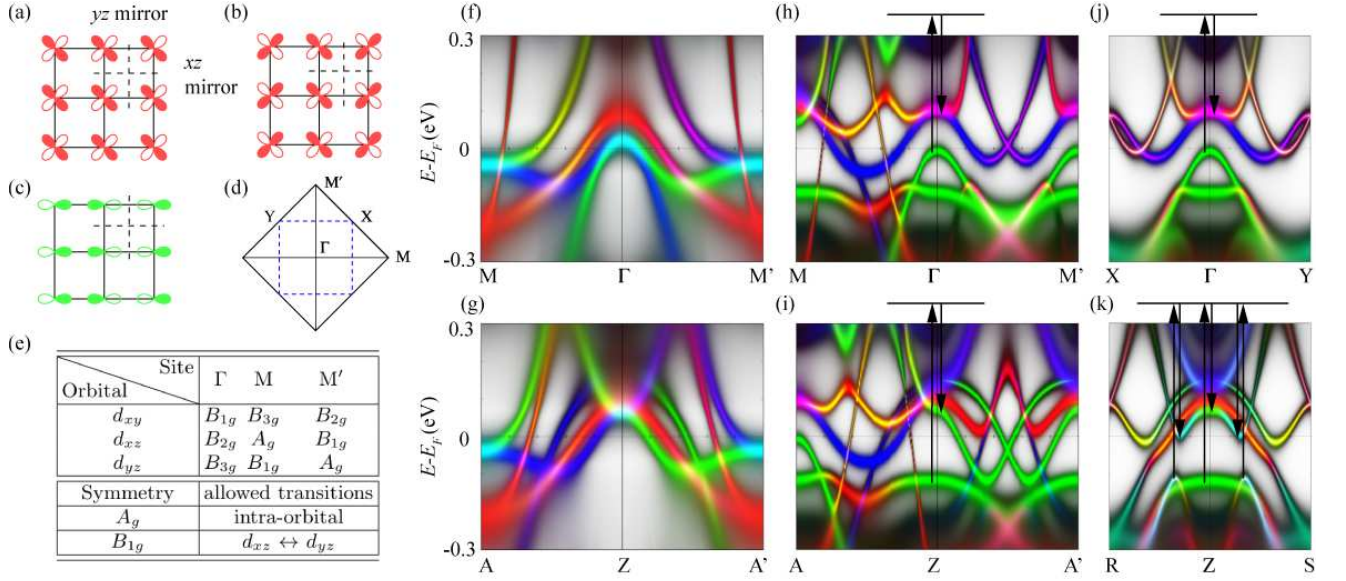


FIG. 3. (Color online) (a)-(c) Schematic representations of Fe 3d orbitals in real space for the high-symmetry points in the reciprocal space: (a)  $d_{xy}$  at  $\Gamma$ , (b)  $d_{xy}$  at M and (c)  $d_{xz}$  at M. Filled and empty lobes represent the sign of the wave functions. Dashed lines are the  $xz/yz$  mirror planes. (d) High-temperature 2-Fe BZ (solid line) and low-temperature folded BZ (dashed line). (e) Summary of the symmetry of the  $d_{xy}$ ,  $d_{xz}$  and  $d_{yz}$  orbitals and high-symmetry points and scattering selection rules for the  $A_g$  and  $B_{1g}$  channels. (f)-(k) Single-particle spectral function of  $\text{CaFe}_2\text{As}_2$  in the paramagnetic phase ((f) and (g)) and SDW phase ((h)-(k)) along high symmetry lines in the  $k_z = 0$  (top row) and  $k_z = 2\pi/c$  (bottom row) planes. The  $d_{xy}$ ,  $d_{xz}$  and  $d_{yz}$  orbital characters are denoted in red, green and blue, respectively.

sample slowly cooled down. The coherence peak around  $1220 \text{ cm}^{-1}$  only appears in the  $XY$ ,  $xx$  and  $yy$  polarization spectra at low temperature. Moreover, a large anisotropy of intensity for this coherence peak is observed between the  $xx$  and  $yy$  polarizations, even though they share the same low-frequency phonon spectra and high-frequency response. Indeed, the intensity of the peak in the  $yy$  polarization is less than half of that in the  $xx$  polarization, and the frequency is slightly higher. In addition, for the  $XX$  and  $xy$  polarizations, we distinguish clearly a smaller feature at  $830 \text{ cm}^{-1}$  that has not been reported in previous Raman studies.

We now switch to our results on  $\text{EuFe}_2\text{As}_2$ . Although we did not succeed in detwinning completely the sample using the same cooling procedure, similar physics is observed. The normal state spectra in the  $XX$  and  $XY$  configurations are very similar to those obtained on  $\text{CaFe}_2\text{As}_2$ . As with  $\text{CaFe}_2\text{As}_2$ , a strong coherence peak is also detected in  $\text{EuFe}_2\text{As}_2$  under the  $XY$  and  $xx$  (or  $yy$ ) configurations, albeit for a slightly smaller peak frequency ( $1060 \text{ cm}^{-1}$ ). In order to confirm the Raman nature of the features observed, we measured Raman spectra on the same sample using a  $476 \text{ nm}$  laser excitation. The results, displayed in Figs. 2(c1)-2(c4), show different backgrounds as compared to the ones recorded with  $647 \text{ nm}$  light. In particular, the broad peak found at  $1800 \text{ cm}^{-1}$  and  $3200 \text{ cm}^{-1}$  in the  $647 \text{ nm}$  spectra are absent in the  $476 \text{ nm}$  spectra, suggesting that they possibly correspond to luminescence signals. Interestingly, the

smaller feature found in  $\text{CaFe}_2\text{As}_2$  using the  $XX$  and  $xy$  polarizations is only present under  $476 \text{ nm}$  excitation.

In order to understand the origin of these electronic Raman excitations, we calculated the band dispersion of  $\text{CaFe}_2\text{As}_2$  by using DFT+DMFT in the paramagnetic and the SDW phases<sup>28</sup>. We used the experimental lattice constants and internal coordinates of the paramagnetic phase. The Coulomb interaction and the Hund's coupling are from Ref.<sup>29</sup>. The band dispersion [single-particle spectral function  $A(k, \omega)$ ] along high-symmetry lines are shown in Figs. 3(f)-(k) with the orbital characters represented by different colors. The high-symmetry points are labeled in Fig. 3(d).

The presence of different gap energies in two different symmetry channels in the SDW phase arises from the complexity of the folded band structures. The band structure near  $E_F$  is dominated by the  $d_{xy}$ ,  $d_{xz}$  and  $d_{yz}$  orbitals of Fe. In the high-temperature phase, there are three hole FSs around the  $\Gamma$  point and two electron FSs around the M point. In the SDW phase the  $d_{xz/yz}$  bands degeneracy is lifted. There is a SDW order induced BZ folding from  $A(\pi/a, 0, 2\pi/c)$  to  $\Gamma$ . At the M ( $M'$ ) point, the two electron bands hybridize with the three folded hole bands from Z ( $\Gamma$ ) and a band gap is opened around M (Z). In contrast to the Dirac node at  $E_F$  reported in  $\text{BaFe}_2\text{As}_2$ <sup>26,27</sup>, the Dirac point in  $\text{CaFe}_2\text{As}_2$  is  $45 \text{ meV}$  above  $E_F$ . Interestingly, there is a second Dirac point at  $E_F$  along the FM direction in the  $k_z = 0$  plane between the  $d_{yz}$  band and the folded  $d_{yz}$  band. In the  $k_z = 2\pi/c$



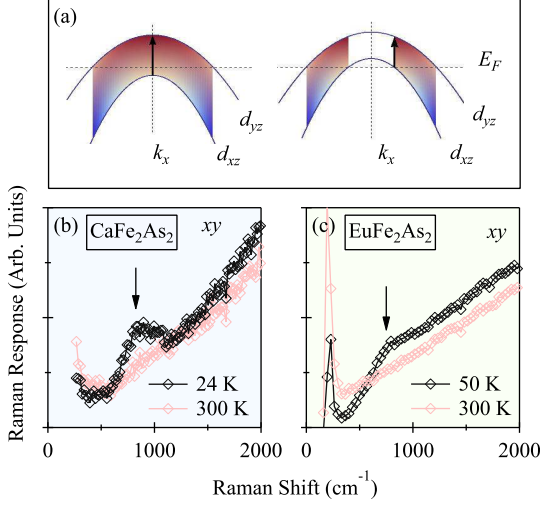


FIG. 4. (Color online) (a) The  $d_{xz}$ - $d_{yz}$  transition at the BZ center and  $k_F$ . The excitations are allowed in the shaded areas. (b) and (c) Differential Raman spectra between 300 K and 24 K (50 K) in  $\text{CaFe}_2\text{As}_2$  and  $\text{EuFe}_2\text{As}_2$ , respectively. The peak in (b) and the threshold in (c), denoted by arrows, correspond to the excitations at the momentum indicated by arrows in (a).

plane, the second Dirac cone carries the  $d_{xz}$  characters and its energy is 36 meV below  $E_F$ .

Raman scattering is a small  $q$  process since the momentum conservation requires the momentum transfer between the initial and final states to be equal to the momentum difference of the scattered and incident lights. As with infrared absorption, the interband electronic Raman scattering intensity is determined by the joint density-of-states and the coherence factor. In the case of non-resonance scattering, the scattering intensity is a reflection of the density-of-states of the initial and final states of the proper symmetry.

The symmetry of the Fe orbitals at the  $\Gamma$  point are defined directly by their corresponding wave functions (Fig. 3(a)). Away from the  $\Gamma$  point though, the phase term  $e^{ik \cdot R}$  in the wave functions can change the parity of some bands<sup>30</sup>. For example, we illustrate in Figs. 3(a) to (c) the  $d_{xy}$  and  $d_{xz}$  orbitals at the M point that changes parity with respect to the  $yz$  mirror plane. At the M point, the parity to the  $xz$  mirror plane is the same as at the  $\Gamma$  point, and the parity to the  $yz$  mirror plane becomes the opposite. Away from high-symmetry points, the situation is more complex and the orbital symmetry is a linear combination of the symmetry at high-symmetry points. We summarize the symmetry of the three dominant orbitals near  $E_F$  in Fig. 3(d). The selection rules between these orbitals are determined by the product of the symmetries of the initial and final states. At the listed high-symmetry points, for the  $A_g$  symmetry channel, only the intraorbital transitions are allowed and for the  $B_{1g}$  symmetry channel, only the  $d_{xz} \leftrightarrow d_{yz}$  transi-

tions are allowed.

While phononic Raman scattering requires as a general selection rule that the symmetry of the phonon states be chosen by the incident and scattered light polarizations, electronic Raman scattering requires more complex selection rules for the symmetry of the initial and final states. The light polarized along the AFM direction ( $x$ ) can excite  $d_{xz}$  bands. For light polarized along the FM ( $y$ ) direction, only  $d_{yz}$  can be excited. Therefore, the peak in the  $xx$  polarization can only arise from  $d_{xz} \leftrightarrow d_{xz}$  transitions. Our calculations further confirm that the  $A_g$  symmetry excitation primarily comes from the Z point, where a band gap opens between the original and the folded  $d_{xz}$  bands (Fig. 3(i)). The second Dirac point in the Z-R and Z-S directions also has a contribution to the Raman spectra (Fig. 3(k)). Since the second Dirac cone contains  $d_{yz}$  components, the scattering for  $yy$  polarization is not fully prohibited.

The small feature in the  $B_{1g}$  channel arises from the  $d_{xz} \leftrightarrow d_{yz}$  transition at the  $\Gamma$  point. We illustrate in Fig. 4(a) this transition for two different levels of  $E_F$ . When the  $d_{xz}$  band is totally below  $E_F$ , the transition will undergo at the BZ center, where the density-of-states is maximum, resulting in a strong scattering signal. This situation is met at the  $\Gamma$  point (Fig. 4(b) and (c))<sup>31,32</sup>. In contrast, when the  $d_{xz}$  band crosses  $E_F$ , the minimum energy transfer is at the momentum wave vector  $k_F$ . In this situation, the spectrum shows a threshold at this minimum energy.

Interestingly, the Raman data are consistent with the  $d_{xz}/d_{yz}$  splitting estimated from ARPES data<sup>9,32</sup>, thus reinforcing its interpretation. Unlike ARPES though, which can access the unoccupied states only for a very small energy range, polarized electronic Raman scattering allows to probe directly the  $d_{xz}/d_{yz}$  splitting at the  $\Gamma$  point, across  $E_F$ .

In conclusion, we reported temperature-dependent and polarization-resolved Raman scattering on twinned  $\text{CaFe}_2\text{As}_2$  and  $\text{EuFe}_2\text{As}_2$  and detwinned mono-domain  $\text{CaFe}_2\text{As}_2$  single-crystals. Two spectral features are observed in two different symmetry channels in the SDW phase. Based on symmetry arguments and DFT+DMFT calculations of the orbital-resolved electronic band structure, we identified these transitions. In the  $A_g$  symmetry channel, there is a spectral weight transfer from low-frequency and the formation of a coherence peak around 1200  $\text{cm}^{-1}$ , which arises from the SDW band-folding-induced intra-orbital transition at the Z point and near the second Dirac point. Moreover, the coherence peak is anisotropic for light polarizations along the AFM and FM directions in detwinned  $\text{CaFe}_2\text{As}_2$ , directly revealing the inequivalent occupancy of the  $d_{xz}$  and  $d_{yz}$  orbitals. In the  $B_{1g}$  symmetry channel, a Raman scattering peak around 800  $\text{cm}^{-1}$  arises from a transition between  $d_{xz}$  and  $d_{yz}$  at the  $\Gamma$  point and reveals the lifted degeneracy of these two orbitals.

W.-L.Z. acknowledges ICAM (NSF-IMI grant DMR-0844115) and NSF (DMR-1104884). P.R. and H.D. ac-

knowledge MoST (2011CBA001001, 2015CB921301) and NFSC (11274362) of China. Z.P.Y. acknowledges NSF DMR130814. Z.B. acknowledges the NCN, Poland (grant no. 2011/01/B/ST5/06937). A.S.S. and G.B. acknowl-

edge the US DOE, BES and Division of Materials Sciences and Engineering under Awards to ORNL and DE-SC0005463 correspondingly.

- 
- \* [girsh@physics.rutgers.edu](mailto:girsh@physics.rutgers.edu)
- <sup>1</sup> G. R. Stewart, *Rev. Mod. Phys.* **83**, 1589 (2011).
  - <sup>2</sup> D. Kasinathan, A. Ormeci, K. Koch, U. Burkhardt, W. Schnelle, A. Leithe-Jasper, and H. Rosner, *New J. Phys.* **11**, 025023 (2009).
  - <sup>3</sup> M. A. Tanatar, A. Kreyssig, S. Nandi, N. Ni, S. L. Bud'ko, P. C. Canfield, A. I. Goldman, and R. Prozorov, *Phys. Rev. B* **79**, 180508 (2009).
  - <sup>4</sup> J.-H. Chu, J. G. Analytis, K. De Greve, P. L. McMahon, Z. Islam, Y. Yamamoto, and I. R. Fisher, *Science* **329**, 824 (2010).
  - <sup>5</sup> A. Dusza, A. Lucarelli, F. Pfuner, J.-H. Chu, I. R. Fisher, and L. Degiorgi, *Europhys. Lett.* **93**, 37002 (2011).
  - <sup>6</sup> M. Nakajima, S. Ishida, Y. Tomioka, K. Kihou, C. H. Lee, A. Iyo, T. Ito, T. Kakeshita, H. Eisaki, and S. Uchida, *Phys. Rev. Lett.* **109**, 217003 (2012).
  - <sup>7</sup> S. Jiang, H. S. Jeevan, J. Dong, and P. Gegenwart, *Phys. Rev. Lett.* **110**, 067001 (2013).
  - <sup>8</sup> S. Kasahara, H. Shi, K. Hashimoto, S. Tonegawa, Y. Mizukami, T. Shibauchi, K. Sugimoto, T. Fukuda, T. Terashima, A. H. Nevidomskyy, *et al.*, *Nature* **486**, 382 (2012).
  - <sup>9</sup> M. Yi, D. Lu, J.-H. Chu, J. G. Analytis, A. P. Sorini, A. F. Kemper, B. Moritz, S.-K. Mo, R. G. Moore, M. Hashimoto, W.-S. Lee, Z. Hussain, T. P. Devereaux, I. R. Fisher, and Z.-X. Shen, *Proc. Natl. Acad. Sci. USA* **108**, 6878 (2011).
  - <sup>10</sup> M. A. Tanatar, E. C. Blomberg, A. Kreyssig, M. G. Kim, N. Ni, A. Thaler, S. L. Bud'ko, P. C. Canfield, A. I. Goldman, I. I. Mazin, and R. Prozorov, *Phys. Rev. B* **81**, 184508 (2010).
  - <sup>11</sup> J.-H. Chu, J. G. Analytis, D. Press, K. De Greve, T. D. Ladd, Y. Yamamoto, and I. R. Fisher, *Phys. Rev. B* **81**, 214502 (2010).
  - <sup>12</sup> T. P. Devereaux and R. Hackl, *Rev. Mod. Phys.* **79**, 175 (2007).
  - <sup>13</sup> T. P. Devereaux and D. Einzel, *Phys. Rev. B* **51**, 16336 (1995).
  - <sup>14</sup> M. Le Tacon, A. Sacuto, A. Georges, G. Kotliar, Y. Gallais, D. Colson, and A. Forget, *Nature Phys.* **2**, 537 (2006).
  - <sup>15</sup> Y. Gallais, R. M. Fernandes, I. Paul, L. Chauvière, Y.-X. Yang, M.-A. Méasson, M. Cazayous, A. Sacuto, D. Colson, and A. Forget, *Phys. Rev. Lett.* **111**, 267001 (2013).
  - <sup>16</sup> Y.-X. Yang, Y. Gallais, R. M. Fernandes, I. Paul, L. Chauvière, M.-A. Méasson, M. Cazayous, A. Sacuto, D. Colson, and A. Forget, *JPS Conf. Proc.* **3**, 015001 (2014).
  - <sup>17</sup> F. Kretzschmar, T. Böhm, U. Karahasanović, B. Muschler, A. Baum, D. Jost, J. Schmalian, S. Caprara, M. Grilli, C. Di Castro, J. G. Analytis, J.-H. Chu, I. R. Fisher, and R. Hackl, ArXiv e-prints (2015), [arXiv:1507.06116](https://arxiv.org/abs/1507.06116).
  - <sup>18</sup> V. K. Thorsmølle, M. Khodas, Z. P. Yin, C. Zhang, S. V. Carr, P. Dai, and G. Blumberg, ArXiv e-prints (2014), [arXiv:1410.6456](https://arxiv.org/abs/1410.6456).
  - <sup>19</sup> W.-L. Zhang, P. Richard, H. Ding, A. S. Sefat, J. Gillett, S. E. Sebastian, M. Khodas, and G. Blumberg, ArXiv e-prints (2014), [arXiv:1410.6452](https://arxiv.org/abs/1410.6452).
  - <sup>20</sup> L. Chauvière, Y. Gallais, M. Cazayous, M. A. Méasson, A. Sacuto, D. Colson, and A. Forget, *Phys. Rev. B* **84**, 104508 (2011).
  - <sup>21</sup> G. Kotliar, S. Y. Savrasov, K. Haule, V. S. Oudovenko, O. Parcollet, and C. A. Marianetti, *Rev. Mod. Phys.* **78**, 865 (2006).
  - <sup>22</sup> K. Haule, C.-H. Yee, and K. Kim, *Phys. Rev. B* **81**, 195107 (2010).
  - <sup>23</sup> M. Matusiak, Z. Bukowski, and J. Karpinski, *Phys. Rev. B* **81**, 020510 (2010).
  - <sup>24</sup> A. S. Sefat, R. Jin, M. A. McGuire, B. C. Sales, D. J. Singh, and D. Mandrus, *Phys. Rev. Lett.* **101**, 117004 (2008).
  - <sup>25</sup> G. Blumberg, R. Liu, M. V. Klein, W. C. Lee, D. M. Ginsberg, C. Gu, B. W. Veal, and B. Dabrowski, *Phys. Rev. B* **49**, 13295 (1994).
  - <sup>26</sup> P. Richard, K. Nakayama, T. Sato, M. Neupane, Y.-M. Xu, J. H. Bowen, G. F. Chen, J. L. Luo, N. L. Wang, X. Dai, Z. Fang, H. Ding, and T. Takahashi, *Phys. Rev. Lett.* **104**, 137001 (2010).
  - <sup>27</sup> N. Harrison and S. E. Sebastian, *Phys. Rev. B* **80**, 224512 (2009).
  - <sup>28</sup> Z. P. Yin, K. Haule, and G. Kotliar, *Nature Phys.* **7**, 294 (2011).
  - <sup>29</sup> Z. P. Yin, K. Haule, and G. Kotliar, *Nature Mater.* **10**, 932 (2011).
  - <sup>30</sup> V. Brouet, M. F. Jensen, P.-H. Lin, A. Taleb-Ibrahimi, P. Le Fèvre, F. Bertran, C.-H. Lin, W. Ku, A. Forget, and D. Colson, *Phys. Rev. B* **86**, 075123 (2012).
  - <sup>31</sup> T. Kondo, R. M. Fernandes, R. Khasanov, C. Liu, A. D. Palczewski, N. Ni, M. Shi, A. Bostwick, E. Rotenberg, J. Schmalian, S. L. Bud'ko, P. C. Canfield, and A. Kaminski, *Phys. Rev. B* **81**, 060507 (2010).
  - <sup>32</sup> P. Richard, C. Capan, J. Ma, P. Zhang, N. Xu, T. Qian, J. D. Denlinger, G.-F. Chen, A. S. Sefat, Z. Fisk, and H. Ding, *J. Phys.: Condens. Matter* **26**, 035702 (2014).